J Mater Sci
DOI 10.1007/s10853-010-4477-5

ICAM 2009

Atomistic study of vibrational properties of γ-Al_2O_3

Claudia Loyola · Eduardo Menéndez-Proupin · Gonzalo Gutiérrez

Received: 26 November 2009 / Accepted: 5 April 2010

Abstract A study of the vibrational density of states (DOS) of γ-Al_2O_3 is presented. Four structural models from the recent literature are considered: vacant spinel model and three nonspinel models. The vacant spinel and one of the nonspinel models have unit cells with 40 atoms, while the other two models have 160 atoms. The interatomic interactions are computed using classical force fields that include Coulomb and van der Waals attractive interactions, short range repulsive interactions, as well as three-body terms. The oxygen polarizability is included via a core-shell potential. The DOS is compared with ab initio calculations recently published for the vacant spinel model. The classical and ab initio DOS show some differences for frequencies higher than 200 cm^{-1}, the ab initio having more peaks and having a frequency cutoff 100 cm^{-1} lower than the classical DOS. The DOS of all models present some small differences. While the 160-atoms nonspinel models present a rather structureless DOS, 40-atoms models present peaks and dips relative to the 160-atoms models. The elastic constants of polycrystalline γ-Al_2O_3 are also estimated using several force fields. In general, the classical force field predict higher elastic moduli than the ab initio method. The infrared spectra of the four models are calculated.

C. Loyola · E. Menéndez-Proupin (✉) · G. Gutiérrez
Departamento de Física, Facultad de Ciencias, Universidad de Chile, Las Palmeras 3425, Ñuñoa, 780-0024 Santiago, Chile
e-mail: eariel99@gmail.com

C. Loyola
e-mail: claudial.81@gmail.com

G. Gutiérrez
e-mail: gonzalo@fisica.ciencias.uchile.cl

Introduction

γ-alumina (γ-Al_2O_3) is the first of the series of transition aluminas, obtained by dehydration of γ-AlOOH at 300–500 °C. The series is followed by δ- and θ-alumina at higher temperatures, to reach the thermodynamically stable phase α-Al_2O_3. γ-Al_2O_3 is the most prominent of the transition aluminas due to its applications as catalyst and catalytic support [1]. It is also applied for structural composites in spacecraft, and abrasive and thermal coatings [2]. In nanocrystalline form, γ-Al_2O_3 is more stable than α-Al_2O_3 due to its lower surface energy [3].

The crystalline structure of γ-Al_2O_3 has been object of debate for many years. The reason is the impossibility to obtain pure single crystals, but a porous material with several possible structures, possibly coexisting as a mixture. Traditionally, it has been regarded as a defective cubic spinel of formula AB_2O_4, where A = B = Al. The spinel structure is depicted in Fig. 1. The O atoms at 32*e* Wyckoff sites form a fcc sublattice. A and B atoms occupy the tetrahedral and octahedral interstices, with Wyckoff positions 8*a* and 16*d*, respectively. There are unoccupied interstices in the structure, at tetrahedral 8*b* and 48*f*, and octahedral 16*c* sites. Hence, A atoms occupy 1/8 of the tetrahedral sites, and B atoms occupy 1/2 of the octahedral sites.

The unit cell of Fig. 1 contains four primitive cells (Al_6O_8). The stoichiometry Al_2O_3 is achieved building triple primitive cells ($Al_{18}O_{24}$) and making 2 Al vacancies. Computational simulation supports models with unit cells of 40 atoms ($Al_{16}O_{24}$), where the spinel lattice has two Al vacancies at octahedral sites at positions that maximize their distances [4–9]. These are the spinel models of γ-alumina, and one of the possible unit cells is shown at Fig. 2d.

Published online: 21 April 2010

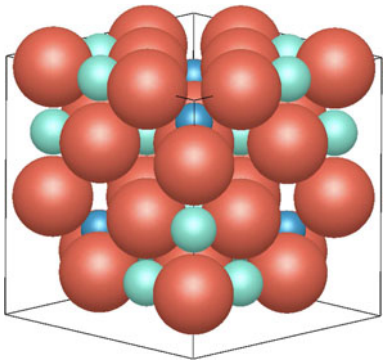

Fig. 1 (Color online) Spinel structure AB_2O_4. Big red spheres are O atoms at 32*e* Wyckoff sites, blue small spheres are A atoms at tetrahedral 8*a* sites, green small spheres are B atoms at octahedral 16*d* sites

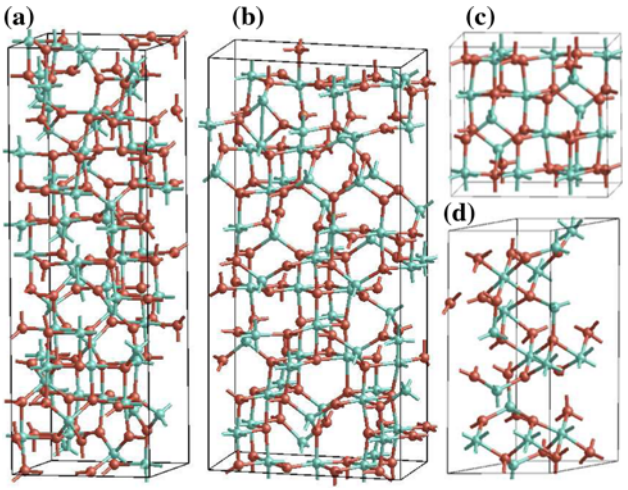

Fig. 2 (Color online) Unit cells of the different structural models of γ-alumina. The structures are the Paglia et al. $Fd\bar{3}m$ (**a**) and $I4_1/amd$ (**b**) models [12, 13], the Krokidis et al. $S_{0,25}$ model (**c**) [14, 15], and the spinel model (**d**) [5, 9]

Neutron diffraction data are better fitted using nonspinel models with the space groups $Fd\bar{3}m$ and $I4_1/amd$ [2, 10, 11]. The space group $Fd\bar{3}m$, is the same of the spinel lattice, but in these alternative structures, some Al atoms occupy different Wyckoff sites. These structures, defined with small unit cells with fractional occupation numbers, do not allow atomistic simulation.

Using a hierarchy of geometric analysis and total energy calculations using classical force fields and ab initio calculations, Paglia et al. [12] explored approximately 1.47 billion of structures where the Al cations are distributed at 8*a*, 16*c*, and 16*d* positions, restricting the relative site occupancies to the proportion obtained from Rietveld refinement of neutron scattering data [2, 11], as well as the lattice parameters. The Al–Al repulsion due to the close proximity of 16*c* and 8*a* sites causes that during the relaxation some Al atoms migrate to other Wyckoff sites (mostly to 48*f*). In this way, Paglia et al. found theoretical minimum energy structures that achieve the best agreement with the experimental diffraction patterns. The obtained structures provide simulated diffraction patterns in better agreement with the experiments than the spinel models. Paglia has published the atomic coordinates in 160-atoms supercells of both the $Fd\bar{3}m$ and $I4_1/amd$ space groups [13], that are depicted in Fig. 2a and b. The symmetry of these models is locally broken due to variations in cation occupancies and related distortions in octahedra and tetrahedra, hence the symmetry of the model structures is really P1.

A different model was obtained by Krokidis et al. [14]. Krokidis et al. proposed a model for dehydration of boehmite, supported by molecular dynamics and DFT calculations. This model describes transformations of a boehmite supercell (16AlOOH) into a spinel-like structure ($Al_{16}O_{24}$) releasing eight water molecules. The water molecules are formed from hydrogen transfers between the adjacent hydroxyl groups. The water extraction leaves deprotonated oxygens and dehydroxylated aluminums in adjacent layers, which link together by a mechanism of structural collapse and shearing. The resulting structure have a fcc oxygen network, with all cations located in octahedral interstices, and one cation vacancy per each Al_2O_3 unit. Cation migration toward tetrahedral interstices completes the transition to a spinel-like structure. The structure with minimal free energy was found to have 25% of cations in tetrahedral sites. This structure is depicted in Fig. 2c, and it is named $S_{0,25}$ (the subindices indicate the % of water and the % of cations in tetrahedral sites in the family of structures studied by Krokidis et al.). The atomic coordinates of the structure $S_{0,25}$ has been published in [15].

The $I4_1/amd$ model achieves the best fit to neutron diffraction data and atomic pair distribution functions obtained from synchrotron X-ray [16] and must be regarded as the best available structural model. The $S_{0,25}$ and the spinel models fit the same data with similar quality, but inferior quality compared with the 160-atoms models [16]. This fact does not rule out completely the less favored models. Tsybulya and Kryukova [17] have simulated the effects of planar defects present in the X-ray diffraction patterns and have argued that spinel-like γ-alumina models with several types of coexisting planar defects can potentially fit the experimental diffraction patterns. On the other hand, Digne et al. [18] claim that the $S_{0,25}$ model provides the best compromise between 40-atoms unit cells and experimental γ-alumina properties, such as the bulk modulus. The bulk modulus of the spinel model has been calculated by Ching et al. [19]. It is higher than the experimental value, and it deviates more than the value obtained for the $S_{0,25}$ model [15]. However, the local density approximation (LDA) used by Ching et al. is known to produce higher bulk moduli than the generalized

gradient approximation (GGA) used by Digne et al. Hence, it is desirable to perform a calculation on both models using the same method.

It has been shown that both spinel and nonspinel models present almost the same electronic structure [9, 15], while it is significantly different from other phases of alumina [19]. It is interesting to compare the vibrational properties of the different models. Vibrational properties are important to uncover dynamical instabilities, for thermodynamical properties, infrared and Raman spectroscopy, etc. There is a recent ab-initio calculation of the phonon structure of the vacant spinel model [19]. That work is based on the structure published in [9], which is equivalent to other structures published elsewhere [5–8, 20, 21]. However, the vibrational properties of the nonspinel models have not been studied yet.

In this study, we present force field calculations of the phonons in γ-alumina using both the spinel [9] and nonspinel [13, 14] models. For the spinel model, we compare the results obtained using different force fields with the ab initio calculation of [19]. We also show a comparison of the elastic constants of the different structures and force fields. Finally, we compare the vibrational densities of states and infrared spectra of the four structural models.

This article is organized as follows. In Sec. 2, we describe the force fields and the method to obtain the vibrational density of states (DOS). In Sec. 3, we present the results of the simulations. In Sec. 4, we present our conclusions.

Computational model

We calculate the vibrational properties using the General Utility Lattice Package (GULP) [22]. The structures are always optimized relaxing the atomic coordinates and the cell parameters. The total energy and the interatomic forces were calculated using classical force fields defined in libraries included in the GULP distribution. In this work, we have used the force fields published in [23] and [24], which we refer as CATLOW and STREITZMINTMIRE libraries, respectively.

The CATLOW library includes short range repulsive and van der Waals attractive interactions by means of a Buckingham potential between atoms i and j

$$U_{ij}(r) = A_{ij}e^{-r_{ij}/\rho_{ij}} - \frac{C_{ij}}{r_{ij}^6}. \quad (1)$$

Also are included the Coulomb interaction using the Ewald method, and oxygen polarizability with the shell model. In the shell model, a spherical massless shell is coupled to the nucleus (core) by a harmonic potential

$$U_{\text{core-shell}}(\Delta r) = \frac{1}{2}k\Delta r^2, \quad (2)$$

where Δr is the distance between the core and the shell center. Only oxygen atoms have shells in the CATLOW library. The potential (1) acts between oxygen shells and between oxygen shells and Al cores, and the Coulomb potential acts between all the components. The parameters are published in [9]. This is the force field used in the study made by Paglia et al. [12], and also in a study of vibrational properties [25] of α-alumina that showed a remarkable agreement with neutron experiments. The CATLOW library also includes three-body angular terms

$$U_{\text{O-Al-O}} = \frac{1}{2}k_2(\theta_{\text{O-Al-O}} - \theta_0)^2, \quad (3)$$

where $\theta_{\text{Ol-Al-O}}$ is the angle between two O shells with Al at the vertex, $\theta_0 = 109.47°$, and $k_2 = 2.09724$ eV/rad^2. This potential becomes zero when Al–O and O–O distances gets larger than 1.9 and 3.5 Å, respectively. This abrupt cutoff causes problems with the geometry optimization due to fluctuations of interatomic distances around the cutoff radii. This was probably the reason not to use this term in the computational study of Ref. [12]. We show below that the three-body term has noticeable effects in the vibrational properties. We name CATLOW0 the force field without the three-body terms.

The library STREITZMINTMIRE is a method developed specifically for Al_2O_3, that includes Buckingham potential, the Coulomb interaction with variable charges, charge transfer energy, and many-body terms. The atomic charges are obtained for each configuration of atomic positions by minimizing the total energy with respect to the charge of each atom, somehow mimicking the ab initio total energy methods. The method is fully described in [24, 26]. This is the most advanced force field available for Al_2O_3. Regretfully, with this library, GULP can only calculate the phonon frequencies at the Γ point. Hence, with this force field, we only computed the optimized lattice vectors and elastic constants and use it to assess the quality of the data obtained with the CATLOW library.

The phonons with wave vector $\mathbf{k}$ are calculated by diagonalization of the dynamical matrix [27]

$$D_{i\alpha,j\beta}(\mathbf{k}) = \frac{1}{\sqrt{m_i m_j}}\sum_{\mathbf{R}}\frac{\partial^2 U}{\partial u_\alpha(i,\mathbf{0})\partial u_\beta(j,\mathbf{R})}e^{i\mathbf{k}\cdot(\mathbf{R}+\tau_{ji})}, \quad (4)$$

where U is the crystal potential energy, $u_\alpha(i, \mathbf{R})$ is the α component of the displacement of the ith atom at lattice site $\mathbf{R}$ from its equilibrium position, and $\tau_{ji} = \tau_j - \tau_i$ where τ_i are the atomic positions in the supercell. The indices i, j runs over the N atoms of the unit cell, and α, β run over the three cartesian coordinates.

The sum on **R** runs over all the lattice vectors. In GULP, this sum is restricted by the cutoffs of the force fields, with the exception of the long range Coulomb interaction, which is summed by the Ewald method.

The DOS was obtained making a histogram of the phonon frequencies calculated for a dense grid of k-points of the Brillouin zone. For the spinel-model unit cell, we used a $40 \times 40 \times 17$ grid, which is enough to have a converged DOS using histogram bins 5 cm^{-1} wide. This grid is equivalent to a $20 \times 20 \times 17$ grid in the Brillouin zone of a $2 \times 2 \times 1$ supercell, as the one used in [19]. For the 40 atoms nonspinel model, we used a $58 \times 38 \times 40$ grid. For the 160 atoms supercells, we used $28 \times 28 \times 9$ and $20 \times 40 \times 9$ grids for $Fd\bar{3}m$ and $I4_1/amd$ models, respectively. We also present the partial densities of states (PDOS), which are the projections of the DOS onto the Al and O atoms.

Results

Figure 3 shows the DOS and PDOS of the spinel structure, calculated with the CATLOW force field. The DOS shows the power dependence typical of acoustic modes in the range 0–150 cm^{-1}. At 160 cm^{-1} appears a peak caused by the edge of the acoustic bands. After this peak, the DOS rises steeply to reach a maximum at 240 cm^{-1}, a subsequent minimum around 300 cm^{-1}, and continues with high values until reach a dip at 700 cm^{-1}. All this structure is associated to the oxygen atoms, as shows the oxygen PDOS. Between 700 and 900 cm^{-1} a few weaker bands appear, and the DOS decreases gradually to extinguish near 980 cm^{-1}.

In Fig. 4, we compare the DOS and PDOS of the spinel structure, calculated with the force fields CATLOW, CATLOW0 (i.e., without the three-body term), and the ab initio data of

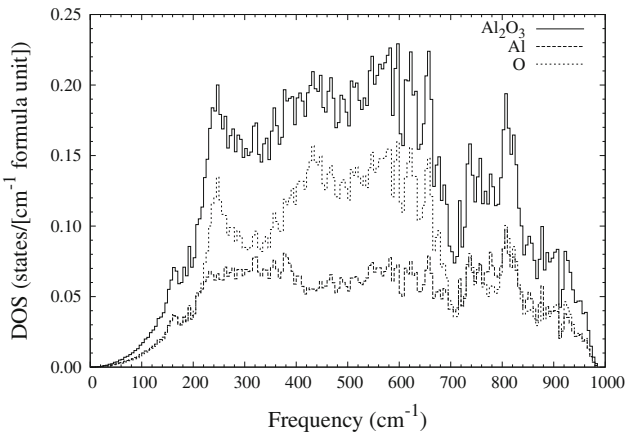

Fig. 3 Vibrational total and partial DOS of spinel model of γ-alumina [9], according to the CATLOW force field

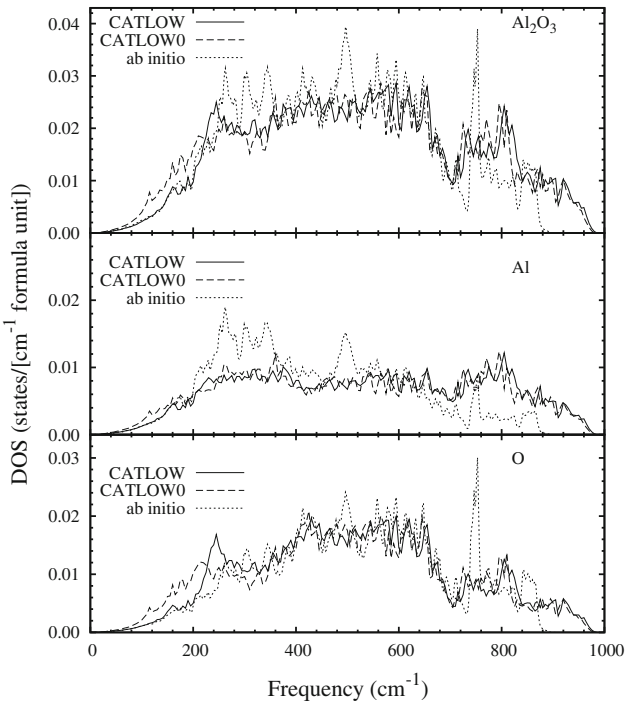

Fig. 4 Comparison of vibrational (total and partial) DOS of γ-alumina (spinel structure [9]), calculated with different force fields and the ab initio data of Ref. [19]

Ching et al. [19]. The lack of three-body O–Al–O interactions in the CATLOW0 force field causes a redshift of DOS edge in the range 0–200 cm^{-1}. The O PDOS has the larger contribution to this effect. In this range, the ab initio DOS is very similar to the CATLOW DOS. In the range 200–360 cm^{-1}, the CATLOW0 shows less states than CATLOW DOS, compensating the increase below 200 cm^{-1}. For higher frequencies, CATLOW and CATLOW0 DOS are rather similar, the latest being slightly redshifted. The ab initio DOS shows large differences for frequencies higher than 200 cm^{-1}, particularly the pronounced bands at 260, 300, 340, 500, and 750 cm^{-1}. According to the PDOS, the first bands at 260, 300, and 340 cm^{-1} are due to Al modes, the band at 750 cm^{-1} is due to O modes, and the band at 500 cm^{-1} has a mixed character. In compensation for the extra modes at these bands, the ab initio DOS extinguishes at 880 cm^{-1}. However, these differences should be regarded with a bit of caution due to methodological differences in the classical and the ab initio calculations. In the classical calculations, the force constants matrix elements are calculated as analytical derivatives of the forces. The force constants decrease with the distance R and become zero after the cutoff radii, allowing a finite number of terms in Eq. 4. In the ab initio calculations with periodic boundary conditions, a supercell is defined, and the force constants matrix elements are calculated by finite differences, moving the atoms of the supercell, once at a time, by a small

distance. Due to the periodic boundary conditions, when an atom of the supercell is moved, it also happens at the periodic images. The consequence is that with a $2 \times 2 \times 1$ supercell [19], the dynamical matrix is found exactly for a $2 \times 2 \times 1$ k-points grid, and for the rest of the k-points used to evaluate the DOS the dynamical matrix is an interpolation. On the other hand, in the GULP calculation, the dynamical matrix was effectively computed on a $40 \times 40 \times 17$ k-points grid.

In Fig. 5, we show a comparison of the phonon DOS of the four structural models, as obtained with the CATLOW force field. The DOS of both 160-atoms nonspinel models are very similar, and show less structure than the DOS of the 40-atoms spinel and nonspinel models. The difference of the spinel model DOS with respect to the 160-atoms nonspinel DOS can be summarized as: (a) peaks at 240, 560, and 800 cm^{-1}, and (b) a dip at 700 cm^{-1} present in the spinel model and absent in the nonspinel models. As can be seen from the PDOS, the differences are principally associated to oxygen vibrations, except the features at 700 and 800 cm^{-1} that have contributions from both O and Al. This is rather surprising, as the O sublattice is the same in both models. Obviously, the Al cations, acting as bridges of the O sublattice, influence the O vibrations more than their own vibrations. The $S_{0,25}$ DOS presents a band between 150 and 195 cm^{-1} and a depletion, relative to the other DOS, between 200 and 300 cm^{-1}, that is associated with oxygen vibrations. Between 400 and 660 cm^{-1} the $S_{0,25}$ DOS have similar values to the spinel model, and higher than the 160-atoms models. Over 870 cm^{-1}, the $S_{0,25}$ DOS is higher than the other DOS, associated with Al vibrations.

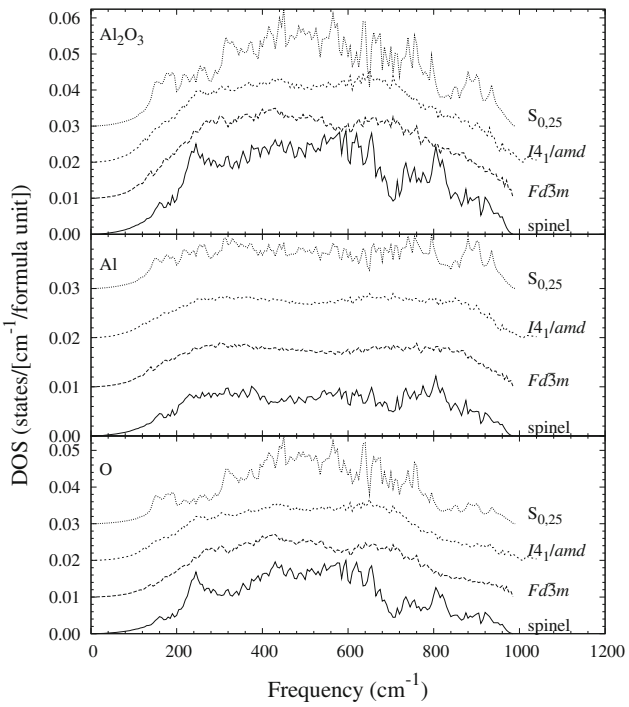

Fig. 5 Comparison of vibrational (total and partial) DOS of different structural models of γ-alumina. The CATLOW force field was used

Table 1 shows the optimized cell parameters and several elastic properties calculated with different methods. The cell parameters obtained with different methods have good agreement between themselves. For the spinel structure, the ab initio lattice vectors are about 1% smaller. However, the CATLOW and CATLOW0 force fields produce more acute cell angles that compensate the larger vectors, giving the same density. There is agreement between the ab initio and force field values of the shear modulus G and the Poisson ratio η, with the exception of the shear modulus obtained with the CATLOW0 library. On the other hand, the bulk modulus B and the Young modulus E are noticeably higher in the force field calculations. In general terms, the STREITZMINTMIRE force field provides the best agreement with the ab initio cell angles and elastic constants. However, let us note that at the Γ point, with the STREITZMINTMIRE library we obtain imaginary frequencies for all the structural models. The STREITZMINTMIRE force field also produces a smaller density. The low shear modulus obtained with the CATLOW0 force field shows the importance of three-body interactions in alumina. We can also compare the elastic properties of the different models as obtained with the same force fields. The spinel structure has higher bulk, shear, and Young moduli than the nonspinel models. In general terms, there is a rather large dispersion in the values of the elastic parameters obtained with the different structural models and force fields.

In Fig. 6, we show the frequency distribution of the zone center phonons ($\mathbf{q} = 0$) and the infrared (IR) spectra of the four model structures. The IR intensities of the vibrational modes are estimated as $I_{IR} \sim (\sum_i q_i d_i)^2$, where i runs for all the species (atom cores and shells), q_i are the charges, and d_i are the cartesian displacements associated with the normalized phonon eigenvectors. The IR envelopes were obtained broadening the discrete lines with Gaussian functions 30 cm^{-1} in width. This Gaussian broadening is intended to simulate the random variations of the phonon frequencies in different parts of the material, rather than to simulate the oscillator spectral lines. This artificial broadening also allows to compare the spectral properties of the 40-atoms models with the 160-atom models, which have a denser spectrum and illustrate how large unit cells are more capable to account for the structural disorder. All models have IR active modes throughout the vibrational spectrum, with maximum intensities in the range 450–750 cm^{-1}. Three of the models present one principal band, in contrast with the $S_{0,25}$ model that presents two well separated bands of almost equal intensities. Experimental IR spectra are somewhat contradictory. Some spectra [28] reveal wide bands in the ranges 500–700 and 700–900 cm^{-1}, while

Table 1 Structural and elastic parameters of γ-Al_2O_3. B, G, E and η are the bulk modulus, shear modulus, average Young modulus, and average Poisson ratio, respectively

Method	a (Å)	b (Å)	c (Å)	α	β	γ	ρ (g/cm^3)	B (GPa)	G (GPa)	E (GPa)	η
Vacant spinel structure [9]											
(a) LDA [19]	5.606	5.570	13.482	89.4°	90.0°	120.2°	3.72	204	113	286	0.266
(b) CATLOW	5.652	5.593	13.372	88.7°	89.9°	120.5°	3.72	279	126	379	0.274
(c) CATLOW0	5.677	5.605	13.267	88.1°	90.0°	120.4°	3.72	264	86	321	0.296
(d) STREITZMINTMIRE	5.669	5.608	13.610	89.1°	90.0°	120.4°	3.63	243	111	343	0.263
Nonspinel structure derived from the $Fd\bar{3}m$ group [13]											
(b) CATLOW	7.908	7.916	23.459	89.9°	90.5°	90.1°	3.69	262	117	258	0.337
(c) CATLOW0	7.935	7.968	23.229	89.1°	91.4°	90.4°	3.69	233	92	212	0.350
(d) STREITZMINTMIRE	8.010	7.955	23.777	90.0°	90.5°	90.3°	3.58	218	101	189	0.359
(e) Experiment [12]	7.911	7.911	23.733	90°	90°	90°	3.65				
Nonspinel structure derived from the $I4_1/amd$ group [13]											
(b) CATLOW	11.147	5.678	23.335	90.1°	89.5°	91.0°	3.67	242	113	316	0.285
(c) CATLOW0	11.121	5.719	22.909	90.4°	89.7°	91.1°	3.72	246	93	257	0.334
(d) STREITZMINTMIRE	11.343	5.726	23.347	90.3°	90.2°	90.0°	3.57	208	94	230	0.318
(e) Experiment (Ref. [12])	11.200	5.600	23.562	90°	90°	90°	3.67				
Nonspinel structure $S_{0,25}$ [15]											
(a) GGA [15]	5.587	8.413	8.068	90.0°	90.59°	90.0°	3.57	171			
(b) CATLOW	5.540	8.380	7.969	90.0°	92.1°	90.0°	3.66	247	123	349	0.259
(c) CATLOW0	5.488	8.382	8.037	90.0°	93.0°	90.0°	3.67	254	103	335	0.275
(d) STREITZMINTMIRE	5.568	8.427	8.019	90.0°	92.0°	90.0°	3.60	204	102	303	0.243
(e) Experiment [15]								162			

B and G are Voigt–Reuss–Hill averages. E are averages along the three axes, and η are averages of η_{ij} for all combinations of directions $i, j = x, y, z$

other spectra [29] show a very broad band between 200 and 1000 cm^{-1}, with small maxima near 340 and 475 cm^{-1} and a shoulder at 800 cm^{-1}. Moreover, some surface and cavity modes may be important in such a porous material like γ-alumina. Considering the contradictions of the experiments, the lack of low temperature measurements that allow more resolution, and the limitations of the structural models, we have limited our discussion to the differences between the theoretical spectra of the different model structures.

Conclusions

We have evaluated the performance of several force fields to calculate the vibrational and elastic properties of γ-Al_2O_3. We have shown that the CATLOW and the more advanced STREITZMINTMIRE force fields, produce elastic constants of the same quality. The Young and bulk moduli obtained with the classical force fields are higher than the values obtained with the ab initio LDA calculation [19].

We show that neglecting the three-body interactions in the CATLOW force field degrades the quality of the shear modulus and produces a redshift in the low frequency edge of the vibrational DOS. The vibrational DOS obtained with the CATLOW force field has a similar shape to the ab initio DOS. The ab initio DOS has more structure, showing pronounced bands at 260, 300, 340, 500, and 750 cm^{-1} at the expense of a dip at 720 cm^{-1} and a high frequency edge at 880 cm^{-1}, which is 100 cm^{-1} lower than for the force fields DOS.

It is not clear if the above-mentioned differences are due to the quality of the force field or to differences in the methodology. In the ab initio calculation [19], the supercell method and the periodic boundary conditions imply that the computed phonon frequencies are strictly correct in a coarse $2 \times 2 \times 1$ k-points grid of the Brillouin zone. The vibrational DOS was calculated with the phonon frequencies in a $20 \times 20 \times 20$ grid of the Brillouin zone. Hence, most of these frequencies are interpolations (via the dynamical matrix) of the frequencies in the coarse grid. To clarify this issue, it is necessary to make force field calculations with the supercell approach used in the LDA calculations. However, this requires additional programs and is beyond our present capabilities.

Finally, assuming that the CATLOW force field produces correct vibrational properties, we have made a comparative study of the DOS and the IR spectra of the spinel model and

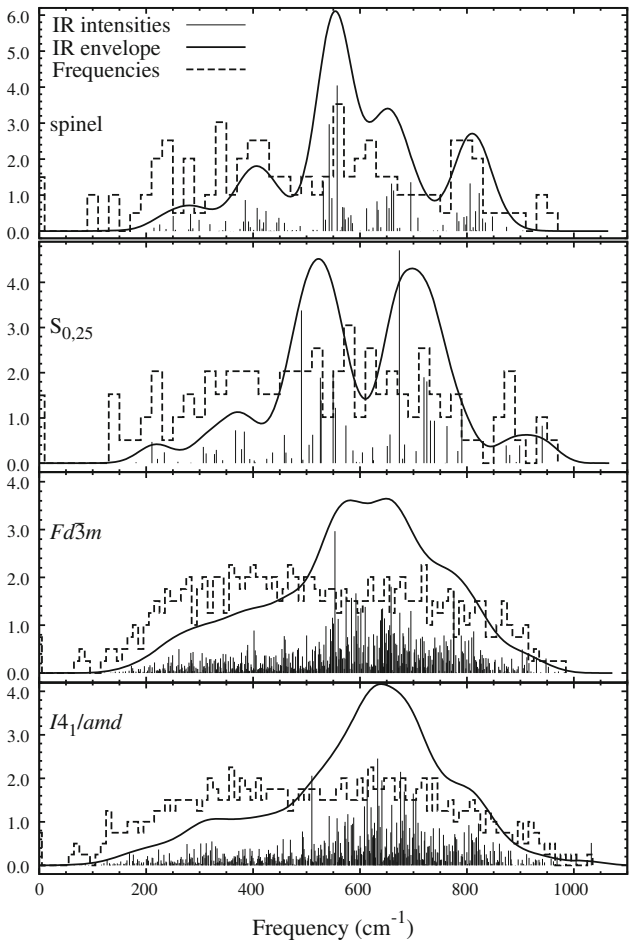

Fig. 6 Infrared spectra simulated with the CATLOW force field. The histogram shows the distribution of the Γ-point phonons

the nonspinel models published by Paglia et al. [12, 13] and by Digne et al. [15]. The DOS of the 160-atoms models are almost unstructured, supporting the claims that γ-Al_2O_3 must be regarded as a random network structure with well defined local order [19]. We have shown that the IR spectra of the four models present significant differences.

Acknowledgements This work was supported by the Chile Bicentennial Program of Science and Technology under Grant no. ACT/ADI-24. We thank Prof. Wai-Yim Ching for useful comments and sharing of the DOS data.

References

1. Wang S, Borisevich AY, Rashkeev SN, Glazoff MV, Sohlberg K, Pennycook SJ, Pantelides S (2004) Nat Mater 3(3):143
2. Paglia G, Buckley CE, Rohl AL, Hunter BA, Hart RD, Hanna JV, Byrne LT (2003) Phys Rev B 68:144110
3. McHale JM, Auroux A, Perrota AJ, Navrotsky A (1997) Science 277:5327
4. Wolverton C, Hass KC (2001) Phys Rev B 63(2):024102
5. Gutiérrez G, Taga A, Johansson B (2002) Phys Rev B 65(1):012101
6. Cai SH, Rashkeev SN, Pantelides ST, Sohlberg K (2002) Phys Rev Lett 89(23):235501
7. Cai SH, Rashkeev SN, Pantelides ST, Sohlberg K (2003) Phys Rev B 67(22):224104
8. Pinto HP, Nieminen RM, Elliott SD (2004) Phys Rev B 70:125402
9. Menéndez-Proupin E, Gutiérrez G (2005) Phys Rev B 72:035116
10. Zhou RS, Snyder RL (1991) Acta Crystallogr Sect B: Struct Sci B 47:617
11. Paglia G, Buckley CE, Rohl AL, Hart RD, Winter K, Studer AJ, Hunter BA, Hanna JV (2004) Chem Mater 16:220
12. Paglia G, Rohl AL, Buckley CE, Gale JD (2005) Phys Rev B 71:224115
13. Paglia G (2004) Determination of the structure of γ-alumina using empirical and first principles calculations combined with supporting experiments. Ph.D. thesis, Curtin University of Technology. Available at http://www.adt.curtin.edu.au/theses/available/adt-WCU20040621.123301/
14. Krokidis X, Raybaud P, Gobichon AE, Rebours B, Euzen P, Toulhat H (2001) J Phys Chem B 105:51213
15. Digne M, Sautet P, Raybaud P, Euzen P, Toulhat H (2004) J Catal 226:54
16. Paglia G, Buckley CE, Rohl AL (2006) J Phys Chem B 110:20721
17. Tsybulya SV, Kryukova GN (2008) Phys Rev B 77:024112
18. Digne M, Raybaud P, Sautet P, Rebours B, Toulhoat H (2006) J Phys Chem B 110:20719
19. Ching WY, Ouyang L, Rulis P, Yao H (2008) Phys Rev B 78:014106
20. Sohlberg K, Pennycook SJ, Pantelides ST (1999) J Am Chem Soc 121:7493
21. Sohlberg K, Pennycook SJ, Pantelides ST (2000) Chem Eng Commun 181:107
22. Gale J, Rohl A (2003) Mol Simul 29:291
23. Catlow CRA, James R, Mackrodt WC, Stewart RF (1982) Phys Rev B 25:1008
24. Streitz FH, Mintmire JW (1994) Phys Rev B 50:11996
25. Rambaut C, Jobic H, Jaffrezic H, Kohanoff J, Fayeulle S (1998) J Phys Condens Matter 10:4221
26. Streitz FH, Mintmire JW (1999) Phys Rev B 60:773
27. Ashcroft NW, Mermin ND (1976) Solid state physics. Harcourt Inc, Orlando, USA
28. Paglia G, Buckley CE, Rohl AL, Hart RD, Jones F, Maitland CF, Connolly J (2004) Chem Mater 16:1914
29. Pecharromán C, Sobrados I, Iglesias JE, González-Carreño T, Sanz J (1999) J Phys Chem B 103:6160